Localization System based on Ultra Low-power Radio Landmarks

Fabian Höflinger[1], Joan Bordoy[2], Rui Zhang[2], Amir Bannoura[1], Nikolas Simon[1], Leonhard Reindl[1] and Christian Schindelhauer[2]

[1]*Department of Microsystems Engineering, University of Freiburg, Germany*

[2]*Department of Computer Science, University of Freiburg, Germany*

Keywords: Indoor Localization, Ultra-wideband, On-demand, Wake-up, Low Power.

Abstract: In this paper we present a novel indoor localization system using external reference landmarks as a guidance system for emergency responders. The landmarks are based on low-power wake-up nodes which can be integrated into smoke detectors. The radio wake-up technology is equipped in the system to extend the lifetime of landmarks. While in sleep mode our landmarks have an overall power consumption of 66 µW making them ready-to-use in case of an emergency for up to 5 years. The landmarks are small and cost-efficient and may be integrated into the building infrastructure. The positioning is achieved by combining the radio ranging and IMU based dead reckoning to overcome the disadvantages of both systems. The experimental results show that the proposed system is able to outperform both standalone systems and meanwhile maintain the low power consumption.

1 INTRODUCTION

In the recent decade, a growing demand in precise indoor locating systems could be observed (Bordoy et al., 2016)-(Kuhn et al., 2009) wireless so that indoor location services, such as locating victims in avalanches or earthquakes, injured skier on ski slope, military personnel, fire fighters or lost children, can be delivered. However, in contrast to this increasing demand, the technology for reliable indoor navigation is still in its infancy, since these applications need very high accuracy requirements, low power consumption and low complexity. Nowadays most of indoor locating technologies can be divided into acoustic, optical, and radio frequency methods. The last type of methods can be divided into continuous wave, for example, WLAN or RFID, and impulse signals. Unfortunately, the above mentioned technologies either cannot fulfill the criteria of high accuracy or low power consumption required by indoor location service applications.

2 STATE-OF-THE-ART

Many non-GPS localization systems based on various technologies have been developed (Fischer and Gellersen, 2010). Most of them can be classified into absolute and relative localization systems.

Absolute localization systems normally require external references that consists of fixed landmarks such as Wi-Fi access points (Bahl and Padmanabhan, 2000) or ultra-wide band systems (Kuhn et al., 2009) to determine the position by measuring the Received Signal Strength Indicator (RSSI) or the Time of Arrival (ToA)/Difference of Arrival (TDoA). Due to its high energy consumption, such systems are required either to be connected to the power grid or frequent battery charging/replacement. As a result, such system are not suitable for catastrophic scenarios due to its high installation costs and power consumption.

The most commonly used relative non-GPS indoor localization approach is inertial measurement units (IMU) based dead reckoning. The IMU can be attached to the body or mount on the shoe of the rescue forces (Höflinger et al., 2013; Zhang et al., 2013; Höflinger et al., 2012; Nilsson et al., 2014). In this approach, the relative positioning is obtained in a recursive manner, i.e. the direction and the distance relative to the initial state are calculated via integration of acceleration and gyroscope data. Therefore, no external reference or pre-installation is needed. The system can also be powered by small size batteries. The main drawback of such systems is that the error will be accumulated over time due to drift of the sensors. Therefore, several approaches have been developed (Zhang et al., 2011), (Fang et al., 2005), (Zhang and Reindl, 2011) to minimize such error. Nevertheless, standalone IMU based localization systems are not capable of providing sufficient accuracy for long term measurements, especially if the nature of move-

Höflinger, F., Bordoy, J., Zhang, R., Bannoura, A., Simon, N., Reindl, L. and Schindelhauer, C.
Localization System based on Ultra Low-power Radio Landmarks.
DOI: 10.5220/0006608800510059
In *Proceedings of the 7th International Conference on Sensor Networks (SENSORNETS 2018)*, pages 51-59
ISBN: 978-989-758-284-4

ments is unsteady, which is often the case during rescue operations.

In order to fulfill the requirements of the indoor location application such as very high accuracy requirements, low power consumption and low complexity, one should decrease the system energy consumption especially for absolute localization systems and increase the tracking accuracy of the system. By applying wake-up technology, the power consumption can be significantly reduced. By combining both absolute and relative localization systems, the tracking accuracy can be greatly enhanced.

3 CONCEPT OVERVIEW

In this paper we present a indoor localization system using landmarks based on low-power wake-up nodes which can be integrated into smoke detectors. As a central component of this system we have developed a handheld device that serves as a master node to communicate with our landmarks. The handheld device broadcasts a wake-up message and measures the Received Signal Strength Indicator (RSSI) of each answer received from all landmarks that woke up. Based on this data the master node calculate the current position of the handheld device.

Furthermore, the handheld device is able to receive inertial sensor data of our wireless IMU which can be integrated in shoes. The additional information allows movement tracking between two wake-up events to increase localization accuracy. Moreover, due to the high short-distance accuracy of inertial data based localization, the number of wake-up events can be reduced and hence lifetime of the reference landmarks is increased.

4 HARDWARE DESIGN

In the following section the main components of the hardware are described:

4.1 Handheld Device

The developed prototype of our handheld device consists of two parts: The credit-card sized low-power computer BeagleBone Black with a compatible touchscreen and our developed expansion circuit board.

As shown in Fig. 1 our developed expansion circuit board. is made up of two wireless modules, a power management module and an EEPROM. One of

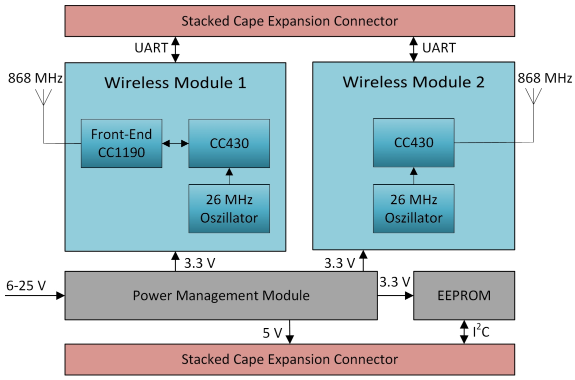

Figure 1: Block diagram of the expansion board with its components. The board is stacked on the BeagleBone Black for communication and power supply (Simon et al., 2015).

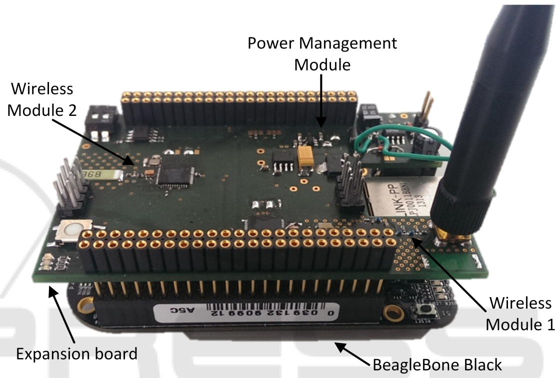

Figure 2: Expansion board stacked on top of the credit-card sized low-power computer BeagleBone Black (Simon et al., 2015).

the wireless modules communicates with our wake-up nodes by transmitting wake-up messages (wake-up message details see Gamm et al. (Gamm et al., 2012)) if requested by the computer and receiving the answers of the landmarks. The other one receives inertial sensor data from our wireless IMU. Both wireless modules use a CC430 low-power microcontroller from Texas Instruments to communicate on a frequency of 868 MHz with the appropriate component. To extend the wake-up range of the system an additional front-end amplifier CC1190 is used for the wireless module. Furthermore, each controller uses a separate UART connection to transfer the received data to the BeagleBone Black computer via the cape expansion connectors.

4.2 Low-power Wake-up Landmarks

Our developed landmarks are based on a wake-up technology presented in Gamm et al. (Gamm et al., 2012) which uses a 125 kHz wake-up receiver. Low power wake-up receivers are used for keyless go entry

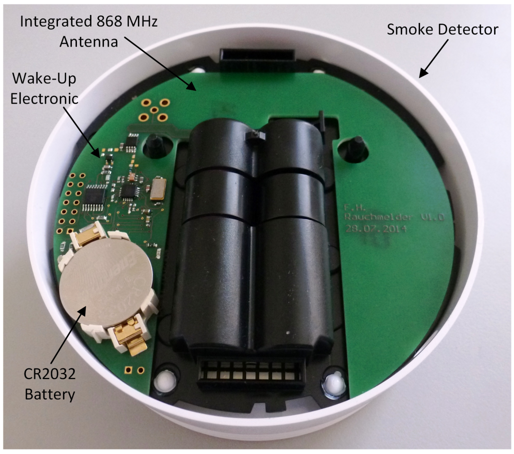

Figure 3: Topview of our developed landmark integrated into a commercially available smoke detector.

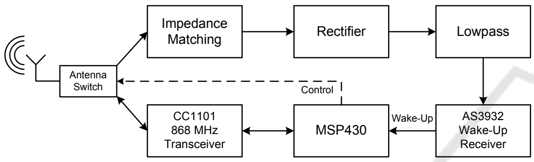

Figure 4: Block diagram of the wake-up circuit in our landmarks (Gamm et al., 2012).

systems in automotives. They are build to work a long time without a battery change and therefore operate at low frequencies. The short wake-up range of about 3 meters due to inductive coupling is of no limiting factor for the keyless go application.

In Fig. 4 a block diagram of the wake-up landmark is shown. When the node is in active mode, the antenna switch is configured so that all in and outgoing signals pass to the main radio transceiver chip. Before entering the sleep mode, the microcontroller toggles the antenna switch. All incoming signals during sleep mode are then routed to the analog circuit consisting of impedance matching, rectifying and low pass filtering. The incoming 868 MHz wake-up signal is passively demodulated by a rectifier and filtered. The passiv demodulation and the analog path is an important factor in the performance of the wake-up receiver since non-ideal impedance matching will result in a shorter wake-up distance. The analog path of the presented node consists of a matching network, two demodulation diodes and a low pass filtering circuit. The RF Schottky demodulator diodes are connected as a typical voltage doubler circuit. Its purpose is to rectify the modulated RF carrier signal. Because of the OOK modulation of the carrier signal the rectifier charges a capacitor of a low pass filter up to a certain value during the ON period of the carrier. When the carrier is turned OFF the capacitor is discharged through a resistor. This way, a triangular signal is generated with a frequency of 125 kHz. Afterwards, the signal is coupled to the wake-up receiver through a capacitor in order to remove any DC offset. The filtered signal is then passed to the input of the wake-up receiver IC. In our node we used the AS3932 wake-up receiver from Austriamicrosystems. It consumes in one channel listening mode 2.7 µA current and has a wake-up sensitivity of 100 µVRMS as well as a high input impedance of 2 MΩ. One of the main reasons for choosing the AS3932 is that it has an integrated correlator which compares the received signal to a byte pattern saved in a configuration register. In case of a positive correlation of the incoming signal with an internal saved 16-Bit sequence the wake-up receiver changes the state of one of its output pins. This signal change is fed to an interrupt capable input port of the microcontroller. The generated interrupt triggers the controller from its sleep to active mode. When entering the active mode, the controller again toggles the antenna switch so that the main radio transceiver is connected to the antenna. The node can then establish a normal communication link, e.g. send an acknowledge or send a message for the RSSI-Measurement between landmark and the handheld device.

While listening for a wake-up packet the standby current of the node is about 2.78 µA which results in a standby power consumption of 5.6 µW. Using a CR2032 coin cell battery with a capacity Q_{Bat} of 230 mAh as power supply we have to take an additional self-discharge current of about 263 nA into account. Therefore, the overall current consumption of the node in sleep mode sums up to 3.044 µA. After the node has been in this mode for t_{sleep} the remaining charge of the battery Q_{Left} can be calculated with the following equation 1. Therefore, the theoretical maximum lifetime of the node without any wake-up is 8.62 years.

$$Q_{Left} = Q_{Bat} - t_{sleep} \cdot I_{sleep} \tag{1}$$

Assuming a maximum current consumption of 15 mA during a sending process which takes about 13 ms the theoretical maximum operating time of our landmarks after t_{sleep} can be calculated using equation 2.

$$T_{maxOp} = \frac{Q_{Left} \cdot T_{Wakeup}}{T_{Send} \cdot I_{Send} + (T_{Wakeup} - T_{Send}) \cdot I_{Sleep}} \tag{2}$$

Once the system is in operation the wake-up period T_{Wakeup} dominates the power consumption and thus the maximum life time of our nodes (Gamm et al., 2012). Figure 5 shows the negative linear be-

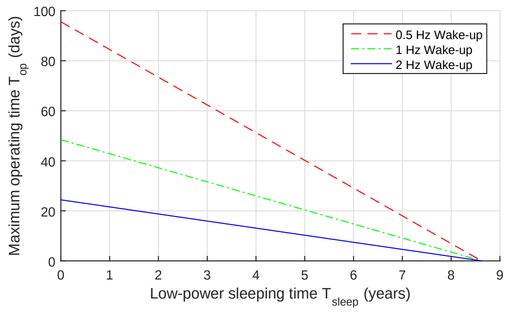

Figure 5: This figure shows the maximum theoretical operating time of a landmark for different wake-up frequencies after it has been in its ultra-low power state for T_{sleep}.

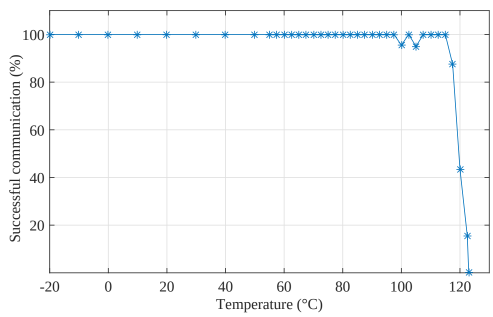

Figure 6: Our measurements show a successful communication within a temperature range of $-20\ °C$ to $115\ °C$.

Table 1: Temperature range of critical components.

	Operating temperature	
Component	**Min. (°C)**	**Max. (°C)**
MSP430F2350	-40	85
CC1101	-40	85
ADG918	-40	85
AS3932	-40	85
HSMS285C	-65	150
Balun 868	-40	125
Crystal	-10	70

haviour of the remaining operating time for three different wake-up periods after the node has been sleeping for t_{sleep}.

As a guidance system for emergency responders the operating temperature range is an important criteria. Table 1 shows that our crystal is the most critical component which limits operation theoretically to a temperature range of $-10\ °C$ to $70\ °C$. However, our practical tests have shown that a successful communication with our nodes is possible within a temperature range of $-20\ °C$ to $115\ °C$ as shown in figure 6. Notice that the radio frequency from the quartz oscillator changes when the temperature varies. Beyond $100\ °C$ the reception bandwidth of receiver can not detect the transmitted radio frequency any more.

With this technology we build a real-time capable low-power landmark with a theoretical maximum standby time which is comparable with the one of commercially available smoke detectors. Therefore, we adapted our circuit board design to be able to integrate the nodes in this extisting infrastructure and hence ease the hardware setup to have a system which is ready-to-use in case of a catastrophic scenario (figure 3).

The sensitivity has been measured in by using a signal generator. A successful wake-up was observed up to an attenuation of -52 dBm (Gamm et al., 2012). Through improved impedance matching a wake-up distance of up to 80 meters is possible at 20 dBm power output (Gamm et al., 2013).

4.3 Micro-inertial Measurement Unit (IMU)

Our wireless micro-IMU V3 (Fehrenbach, 2014) used in this application, has already been successfully used for short-distance indoor motion tracking of pedestrians when mounted on a shoe (Höflinger et al., 2012). With its small size of 22 mm×14 mm× 4 mm the micro IMU is in this application mounted on a shoe and transmits its sampled sensor data wirelessly to our receiver, the handheld device. Concerning this, a CC430 microcontroller from Texas Instruments is used to transmit the data at 868 MHz. Besides the controller the micro IMU consists of a three-axis accelerometer, a three-axis gyroscope and a three-axis magnetometer as well as a voltage regulator (see Fig. 7). The raw data of the sensors can be sent with a maximum rate of 640 samples per second. Thereby, data post processing is done by the receiver to increase the performance of the IMU. More details about metrological characteristics can be found in Höflinger et al. (Höflinger et al., 2012).

5 LOCALIZATION

5.1 Problem Setting

The low power wake-up nodes are placed randomly at unknown stationary positions $\mathbf{S}_j$ $(1 \leq j \leq B)$. For simplicity, we assume they are located in a two-dimensional Euclidean space. The handheld device **H** moves in the two-dimensional Euclidean space, waking up the nodes and measuring the signal strength (RSSI).

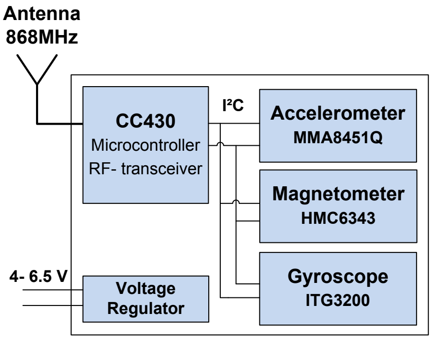

Figure 7: Block diagram of the Micro-IMU V3 (Fehrenbach, 2014). The IMU is capable of transmitting acceleration, magnetic field and angle velocity sensor data via its 868 MHz radio module.

Figure 8: Topview of the micro-IMU V3 which is mounted on a shoe.

5.2 Range Estimation

The handheld device is located at a distance d from the node j:

$$d = \|\mathbf{H} - \mathbf{S}_j\| \tag{3}$$

where $\|\cdot\|$ denotes the Euclidean norm.

The relation between d and the RSSI measurements can be modelled as follows (Qi, 2003):

$$P_R = \frac{G_t G_r}{4\pi} P_T \frac{g^2\gamma}{d^n} \tag{4}$$

where P_T is the transmitted power, G_t and G_r are the transmitter and the receiver gains, respectively, n is the path loss exponent, and g and γ are the parameters that conform the Rayleigh/Rician and lognormal distributions, respectively.

Assuming the received signals are averaged over a certain time interval, the fast fading term can be eliminated. Thus, the logarithmic equation which relates the received signal strength and the distance can be formulated as follows (Qi, 2003) (Mazuelas et al., 2009):

$$P_R(dBm) = \alpha - 10n\log_{10}(d) + \chi \tag{5}$$

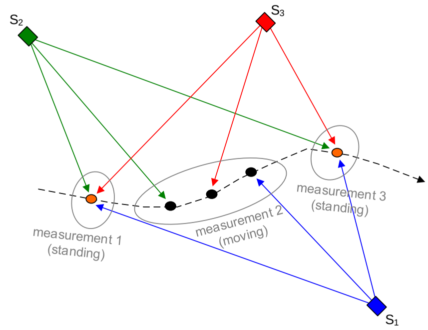

Figure 9: Schematic of the under-determined equation system. If the firefighter moves continuously, for every new measurement there are two new variables to estimate only for its position. On the other hand, if he stops, his device receives one signal from every node (S_1,S_2 and S_3), leading to three constrains for every two position variables (Simon et al., 2015).

where χ denotes a Gaussian random variable with zero mean caused by shadowing. The term α is a constant which depends on the averaged slow and fast fading, the transmitted power and the gains of the antennas.

5.3 Node and Standing Positions Localization

The continuous movement of the master device results in a system of equations which cannot be solved in closed form, as for every received measurement there are two new variables of position to estimate. Consequently, the equation system is underdetermined and cannot be solved in closed form without further information or assumptions on the scenario. Therefore, we assume the master node stops in q different positions $\mathbf{H}_i$, then we have time to receive at least one signal from every node (*stop-and-go motion*). Doing this, it is only required to estimate one handheld device position (2 variables) for every B received signals, which makes possible an uniquely determined system of equations (cf. Fig. 9).

Then, we obtain a system of hyperbolic equations of the form:

$$f_{p,j} = \|\mathbf{H}_p - \mathbf{S}_j\| - z_{p,j} \tag{6}$$

where $1 \leq j \leq B$ and $1 \leq p \leq q$. The term $z_{p,j}$ is the measured distance between the sender j and the standing position p using a RSSI measurement and Equation (5).

The system of equations has now qB independent equations, which has to be higher than the number of

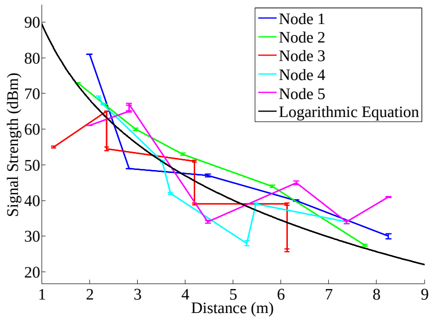

Figure 10: Real and modeled relation between the received signal strength and the distance between the node and the hand-held device. The uncertainty bars show the standard deviation of the signal strength after the 5% highest and the 5% lowest RSSI signals for each distance have been rejected.

variables:

$$qB \geq \underbrace{2q}_{\text{Handheld device}} + \underbrace{2B}_{\text{Nodes}} \tag{7}$$

Which means the system of equations can be solved in a closed form if the number of standing still positions q is higher than:

$$q \geq \frac{2B}{B-2} \tag{8}$$

Assuming the *stop-and-go* motion and having a number of standing positions and nodes fulfilling Equation (8) the system of hyperbolic equations can be solved with local optimization algorithms. We use both the gradient descent and the Gauss-Newton method, the two are first-order methods that use the derivative of the system of hyperbolic error equations. The Equation (6) results in a quadratic objective which can be formulated as follows:

$$\sum_{p=1}^{q} \sum_{j=1}^{B} \underset{\mathbf{H}_p, \mathbf{S}_j}{\arg\min} \, (f_{p,j})^2 \, . \tag{9}$$

Which in vector notation is proportional to $w = \frac{1}{2}\mathbf{b}^T\mathbf{b}$ with $\mathbf{b} = (f_{1,1}, \ldots, f_{q,B})^T$. The operator $(\cdot)^T$ denotes the transposition.

We calculate the direction of the steepest ascent:

$$\nabla w = \nabla \left(\frac{1}{2}\mathbf{b}^T\mathbf{b} \right) = \mathbf{Q}^T\mathbf{b} \tag{10}$$

where $\mathbf{Q}$ is the Jacobian matrix:

$$\mathbf{Q} = \begin{bmatrix} \frac{\partial f_{1,1}}{\partial \mathbf{S}_1} & \cdots & \frac{\partial f_{q,B}}{\partial \mathbf{S}_1} \\ \vdots & \ddots & \vdots \\ \frac{\partial f_{1,1}}{\partial \mathbf{S}_B} & \cdots & \frac{\partial f_{q,B}}{\partial \mathbf{S}_B} \\ \frac{\partial f_{1,1}}{\partial \mathbf{H}_1} & \cdots & \frac{\partial f_{q,B}}{\partial \mathbf{H}_1} \\ \vdots & \ddots & \vdots \\ \frac{\partial f_{1,1}}{\partial \mathbf{H}_q} & \cdots & \frac{\partial f_{q,B}}{\partial \mathbf{H}_q} \end{bmatrix}^T \tag{11}$$

The partial derivative with respect to a vector is defined as the derivative with respect to each of its components:

$$\frac{\partial f_{p,j}}{\partial \mathbf{H}_i} = \left(\frac{\partial f_{p,j}}{\partial H_{p,x}}, \frac{\partial f_{p,j}}{\partial H_{p,y}} \right)^T \tag{12}$$

In our case the partial derivative with respect to the node position S_j is:

$$\frac{\partial f_{p,j}}{\partial \mathbf{S}_j} = -\frac{\mathbf{H}_p - \mathbf{S}_j}{\|\mathbf{H}_p - \mathbf{S}_j\|} \tag{13}$$

The partial derivative with respect to the handheld position is:

$$\frac{\partial f_{p,j}}{\partial \mathbf{H}_p} = \frac{\mathbf{H}_p - \mathbf{S}_j}{\|\mathbf{H}_p - \mathbf{S}_j\|} \tag{14}$$

All the variables which need to be estimated are components of the state vector $\mathbf{u}$:

$$\mathbf{u} = (\mathbf{S}_1^T, \ldots, \mathbf{S}_B^T, \mathbf{H}_1^T, \ldots, \mathbf{H}_q^T)^T \tag{15}$$

Every iteration the state vector is updated using $\mathbf{Q}$ and $\mathbf{b}$. The methods used are:

5.3.1 The Gradient Descent Method

In every iteration step l the Gradient Descent method updates the state vector in direction of the steepest descent. The adaptive factor λ sets the step width.

$$\begin{aligned} \hat{\mathbf{u}} &= \lambda \nabla w = \lambda \mathbf{Q}^T \mathbf{b} \\ \mathbf{u}^{l+1} &= \mathbf{u}^l - \hat{\mathbf{u}} \end{aligned} \tag{16}$$

5.3.2 The Gauss-Newton Algorithm

Instead of relying on an adaptive factor γ it calculates the step size using the inverse $(\mathbf{Q}^T\mathbf{Q})^{-1}$ for every iteration:

$$\mathbf{u} = (\mathbf{Q}^T\mathbf{Q})^{-1}(\mathbf{Q}^T\mathbf{b}) \tag{17}$$

We calculate for higher numerical stability the pseudo-inverse with singular value decomposition instead of calculating the inverse.

This algorithm is faster, nevertheless it is very prone to divergence when applied to random initial positions. However, it can be used when the Gradient Descent error function has become steady to reduce notably the number of iterations (Wendeberg et al., 2013).

5.4 Handheld Device Localization. Data Fusion

The IMU has been proved to be capable of tracking pedestrians in indoor areas showing a maximum deviation of 1 m after a walk of 30 m (Höflinger et al., 2012). However, it cannot be used as the only source of information due to its accumulative error. In order to solve this, we combine the measurements of the IMU and the anchor nodes using an unscented Kalman filter (UKF). The UKF is a recursive state estimator which fulfils the bayesian filtering model and uses a set of sample points (*sigma points*) to linearise non-linear functions. Therefore, it is cheaper in computation than other similar algorithms like the particle filter, which requires evaluation of a large number of particles, or the extended Kalman filter, which requires calculation of the Jacobian matrix. More detailed information about it and its implementation can be found in (Thrun et al., 2005). In our case, the state vector $\mathbf{x}_t$ which contains the variables to estimate has the following components:

$$\mathbf{x}_t = \left(\mathbf{M}_t^T, \mathbf{V}_t^T, \mathbf{A}_t^T\right)^T \tag{18}$$

where $\mathbf{M}_t$ is the position of the target, $\mathbf{V}_t$ his velocity and $\mathbf{A}_t$ the acceleration. All of them in a two-dimensional euclidian space.

We use the the Weiner process acceleration model (Bar-Shalom et al., 2001) in two dimensions.

$$\begin{bmatrix}\mathbf{M}_t\\ \mathbf{V}_t\\ \mathbf{A}_t\end{bmatrix} = \Theta_{t-1}\begin{bmatrix}\mathbf{M}_{t-1}\\ \mathbf{V}_{t-1}\\ \mathbf{A}_{t-1}\end{bmatrix} + \Phi_{t-1} \qquad \Phi_{t-1} \sim \mathcal{N}(0, R_m) \tag{19}$$

where

$$\Theta_t = \begin{bmatrix}1 & \Delta t & \Delta t^2\\ 0 & 1 & \Delta t\\ 0 & 0 & 1\end{bmatrix} \qquad R_m = \tau\begin{bmatrix}\frac{\Delta t^5}{20} & \frac{\Delta t^4}{8} & \frac{\Delta t^3}{6}\\ \frac{\Delta t^4}{8} & \frac{\Delta t^3}{3} & \frac{\Delta t^2}{2}\\ \frac{\Delta t^3}{6} & \frac{\Delta t^2}{2} & \Delta t\end{bmatrix} \tag{20}$$

where τ is a parameter that depends on the expected movement of the target.

In this case we assume each time the nodes are woken up the RSSI measurements are received at the same position. Then, having RSSI measurements of N different nodes at time t, the first N components of the predicted measurement vector $\bar{z}_{t,1:N}$ fulfil the following sensor model:

$$\bar{z}_{t,i} = \alpha - 10n\log_{10}(\|\mathbf{M}_t - \mathbf{S}_i\|) + \rho_t \qquad \rho_t \sim \mathcal{N}(0, \sigma_r) \tag{21}$$

where σ_r is the expected standard deviation of the RSSI measurement noise. We combine these measurements with the foot-mounted IMU measurements. The sensors that we use are the accelerometer and the gyroscope.

We remove the effect of the gravity and extract the x and y components of the acceleration by combining the acceleration and the angular rate. More information about this transformation can be found in (Kuipers, 2002). Then, the components $N+1$ and $N+2$ of the measurement vector are predicted as follows:

$$\bar{z}_{t,N+1:N+2} = \mathbf{A}_t + \nu_t \qquad \nu_t \sim \mathcal{N}(0, \sigma_q) \tag{22}$$

where σ_q is the expected noise of the acceleration measurement.

To reduce the drift of the IMU sensors, we detect when the human being is not moving and we set the velocity and the acceleration to zero, as it is done in (Woodman and Harle, 2008). As the IMU has a much higher sampling rate than the nodes, the sensor data fusion is only done when the velocity and acceleration are not set to zero and there is a RSSI measurement available. In the other cases, the UKF estimates the values using only the IMU measurements.

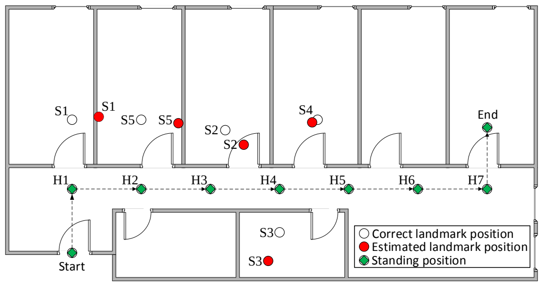

Figure 11: Node localization. The master node stands still in 7 positions $\mathbf{H}_1,\ldots,\mathbf{H}_7$ measuring the signal strength of the nodes $S_1,\ldots,S_5$. These measurements are used as an input of local optimization algorithms (Simon et al., 2015).

6 EXPERIMENTAL RESULTS

6.1 Relation between Signal Strength and Distance

The parameters of the theoretical model which relates the received signal strength and the distance (see Equation (5)) are estimated by collecting measurements from 5 nodes in 7 different positions in a corridor. The best fit to the real measurements are a path loss exponent of 7.1 and a constant α equal to 89.7 (see Fig. 10).

6.2 Node and Standing Positions Localization

In order to test the node localization, we stop in 7 positions $\mathbf{H}_1, \ldots, \mathbf{H}_7$, as shown in Fig. 11. Such positions are assumed to be known, as they can be estimated by

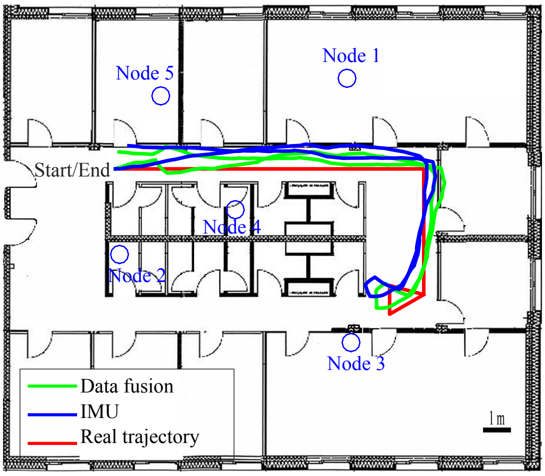

Figure 12: Master node localization. A person moves continuously with the IMU attached to his shoe. Sensor data fusion is performed to combine the RSSI and the IMU data.

the inertial measurement unit, when the accumulative error is still negligible. As the standing positions are symmetrical to the node positions, the local optimization algorithms are initialized on the side of their true value. The resulting median error is 78 cm.

The same data is used to test the hand-held device localization without IMU. The node positions are assumed to be known and the target is located with a median error of 99 cm.

6.3 Continuous Movement Tracking

In order to test the performance of the sensor data fusion we perform an experiment in a different building of the faculty, using the same path loss exponent and α mentioned above. The device was attached to the foot of a person. The sampling rate of the IMU is 50 Hz and data from the wake-up nodes is received every 3 seconds. As having only one RSSI measurement can lead to high errors, the measurement noise of the RSSI measurements is increased in this case in order to reflect this uncertainty. In Fig. 12 we can see both the result of using only the IMU and sensor data fusion. The median error using only the IMU is 0.470 m with a standard deviation of 0.332 m while the median error using also the RSSI measurements is 0.276 m with a standard deviation of 0.229 m. Therefore, the error is notably reduced.

7 CONCLUSION AND FUTURE WORK

In this paper, we have presented a novel self-calibrating indoor localization system for emergency responders using 868 MHz radio landmarks and inertial sensor data. For this system we have developed new wireless landmarks using ultra low-power wake-up technology, which makes them ready-to-use for up to 8 years if powered by a coin cell. The nodes are integrable into building infrastructures like smoke detectors. Moreover, a handheld device has been developed to send initial wake-up calls to the landmarks, measure the RSSI of the response, and use this data to estimate and display the current position of the firefighter. Additionally, our handheld device is able to receive inertial sensor data by a body-mounted micro-intertial measurement unit (IMU) to increase localization accuracy. The data is fused with an Unscented Kalman filter.

The experimental results demonstrate that using the obtained relation of signal strength and distance the system is able to locate our landmarks with a median error of 78 cm in an indoor environment. Moreover, fusing the RSSI and IMU data, the continous trajectory of the firefighter is tracked with a median error of 27.6 cm.

Due to the fact that the RSSI approach is highly sensitive to the environments, long-term high accuracy tracking can not be ensured. In the future, we plan to equip our landmark device with Ultra-Wide-Band (UWB) technology. Instead of measuring the RSS, signal time of arrival will be used as the measurement for improving the localization accuracy. Meanwhile, more reliable estimators that explicitly consider outlier error mitigation, e.g. RANSAC (Bordoy et al., 2016), or robust regression (Bordoy et al., 2017) will be investigated and adapted for the proposed system so that system robustness can be enhanced.

ACKNOWLEDGEMENTS

This work has partly been supported by the German Federal State Postgraduate Scholarships Act (Landesgraduiertenförderungsgesetz - LGFG) within the cooperative graduate school “Decentralized sustainable energy systems".

REFERENCES

Bahl, P. and Padmanabhan, V. N. (2000). Radar: An in-building rf-based user location and tracking system. In *INFOCOM 2000. Nineteenth Annual Joint Conference of the IEEE Computer and Communications Societies. Proceedings. IEEE*, volume 2, pages 775–784. Ieee.

Bar-Shalom, Y., Li, X. R., and Kirubarajan, T. (2001). *Estimation with applications to tracking and navigation*. Wiley-Interscience.

Bordoy, J., Schindelhauer, C., Zhang, R., Höflinger, F., and Reindl, L. M. (2017). Robust extended kalman filter for nlos mitigation and sensor data fusion. In *Inertial Sensors and Systems (INERTIAL), 2017 IEEE International Symposium on*, pages 117–120. IEEE.

Bordoy, J., Wendeberg, J., Schindelhauer, C., Höfflinger, F., and Reindl, L. M. (2016). Exploiting ground reflection for robust 3d smartphone localization. In *Indoor Positioning and Indoor Navigation (IPIN), 2016 International Conference on*, pages 1–6. IEEE.

Fang, L., Antsaklis, P. J., Montestruque, L., McMickell, M. B., Lemmon, M., Sun, Y., Fang, H., Koutroulis, I., Haenggi, M., Xie, M., et al. (2005). Design of a wireless assisted pedestrian dead reckoning system-the navmote experience. *Instrumentation and Measurement, IEEE Transactions on*, 54(6):2342–2358.

Fehrenbach, P. (2014). Entwicklung einer inertialsensorik zur analyse von schwimmbewegungen.

Fischer, C. and Gellersen, H. (2010). Location and navigation support for emergency responders: A survey. *IEEE Pervasive Computing*, 9(1):38–47.

Gamm, G., Kostic, M., Sippel, M., and Reindl, L. M. (2012). Low power sensor node with addressable wake-up on demand capability. *Int. J. Sensor Networks*, 11(1):48–56.

Gamm, G., Sester, S., Sippel, M., and Reindl, L. M. (2013). Smartgate - connecting wireless sensor nodes to the internet. *Journal of Sensors and Sensor Systems*, pages 45–50.

Höflinger, F., Müller, J., Zhang, R., Reindl, L. M., and Burgard, W. (2013). A wireless micro inertial measurement unit (imu). *Instrumentation and Measurement, IEEE Transactions on*, 62(9):2583–2595.

Höflinger, F., Zhang, R., and Reindl, L. M. (2012). Indoor-localization system using a micro-inertial measurement unit (imu). In *European Frequency and Time Forum (EFTF), 2012*, pages 443–447. IEEE.

Kuhn, M., Zhang, C., Lin, S., Mahfouz, M., and Fathy, A. E. (2009). A system level design approach to uwb localization. In *Microwave Symposium Digest, 2009. MTT'09. IEEE MTT-S International*, pages 1409–1412. IEEE.

Kuipers, J. (2002). *Quaternions and Rotation Sequences*. Princeton Paperbacks.

Mazuelas, S., Bahillo, A., Lorenzo, R. M., Fernandez, P., Lago, F. A., Garcia, E., Blas, J., and Abril, E. J. (2009). Robust indoor positioning provided by real-time RSSI values in unmodified wlan networks. *Selected Topics in Signal Processing, IEEE Journal of*, 3(5):821–831.

Nilsson, J.-O., Rantakokko, J., Händel, P., Skog, I., Ohlsson, M., and Hari, K. (2014). Accurate indoor positioning of firefighters using dual foot-mounted inertial sensors and inter-agent ranging. In *Proceedings of the Position, Location and Navigation Symposium (PLANS), 2014 IEEE/ION*.

Qi, Y. (2003). *Wireless geolocation in a non-line-of-sight environment*. PhD thesis, Princeton University.

Simon, N., Bordoy, J., Höflinger, F., Wendeberg, J., Schink, M., Tannhäuser, R., Reindl, L. M., and Schindelhauer, C. (2015). Indoor localization system for emergency responders with ultra low-power radio landmarks. In *International Instrumentation and Measurement Technology Conference (I2MTC)*.

Thrun, S., Burgard, W., and Fox, D. (2005). *Probabilistic Robotics*. mitpress.

Wendeberg, J., Höflinger, F., Schindelhauer, C., and Reindl, L. (2013). Calibration-free TDOA self-localization. *Journal of Location Based Services*.

Woodman, O. and Harle, R. (2008). Pedestrian localisation for indoor environments. In *Proceedings of the 10th international conference on Ubiquitous computing*, pages 114–123. ACM.

Zhang, R., Höflinger, F., Gorgis, O., and Reindl, L. (2011). Indoor localization using inertial sensors and ultrasonic rangefinder. In *Wireless Communications and Signal Processing (WCSP), 2011 International Conference on*, pages 1–5. IEEE.

Zhang, R., Höflinger, F., and Reindl, L. (2013). Inertial sensor based indoor localization and monitoring system for emergency responders. *Sensors Journal, IEEE*, 13(2):838–848.

Zhang, R. and Reindl, L. (2011). Pedestrian motion based inertial sensor fusion by a modified complementary separate-bias Kalman filter. In *Sensors Applications Symposium (SAS), 2011 IEEE*, pages 209–213. IEEE.